



Sensitivity and Optimization Analysis of Torsional Behavior in Multicellular Thin-Walled Tubes

Ammar A. Alshannaq^{1*}, Mohammad F. Tamimi¹, Mu'ath I. Abu Qamar¹

¹ Department of Civil Engineering, Yarmouk University, P.O. Box 566, Irbid 21163, Jordan.

Received 24 June 2024; Revised 10 August 2024; Accepted 16 August 2024; Published 01 September 2024

Abstract

Multicellular thin-walled tubes are widely used due to their lightweight, economical design, and superior shear and torsional performance. Their design is sometimes governed by the available materials and the required dimensions. The current study uses advanced sensitivity analysis with meta-modeling tools to understand how different geometric and mechanical factors affect the torsional performance of multicellular thin-walled tubes. The geometric factors include the length, thickness, and width of the beams, while the mechanical properties involve the shear modulus. Variance-based sensitivity analysis is used to assess how variations in these factors impact the rate of twist, torsional stiffness, and shear stress. The interconnected relations between input parameters are exploited for optimal design and superior performance. The results revealed that for a three-celled tube, thick horizontal interior elements with thin deep vertical elements and thin exterior elements provide an optimal design when the cross-sectional area is constrained. This finding, combined with varying the geometrical and material properties, results in an optimal design using CFRP composites when constrained by minimizing the total weight and superior torsional performance. The analysis can be extended to include other constraint(s), but changing the design constraints might change the optimal design.

Keywords: Multi-Cellular Thin-Walled Structure; Sensitivity; Composites; Torsional Properties; Uncertainty; Optimization.

1. Introduction

Multicellular thin-walled tubes, either open- or closed-sections, have been in use in structural applications for a long time. Their lightweight, economical design and superior performance in terms of reduced shear stresses make them attractive options as compared to their solid counterparts [1, 2]. The torsional properties of such structural members have been studied extensively since the 1980's. Numerous amounts of work have been done on analytical and numerical solutions of such structures under torsion (i.e., solving this statically indeterminate problem to obtain the distribution of shear stresses and deformations) [3-5].

The theory behind such structures has been derived for prismatic members with circular and non-circular cross-sections by the method of mechanics of materials and solved by the elastic-membrane analogy [6]. A solution to such a problem has been obtained by various approaches [7-14]. However, the elastic membrane analogy method cannot be applied to cross-sections with composite materials (i.e., multiple materials used in fabrication of the cross-section resulting from optimization analysis). These composite cross-sections have been used due to their additional reduction in weight and increase in stiffness as compared to their homogenous counterparts [15]. They have been modeled and solved through various approaches in the previous studies [16-23] and implemented on various applications (e.g., wind turbine blades, airplane wings, structural bridge girders, power transmission poles) [24-27].

* Corresponding author: aalshannaq@yu.edu.jo

<http://dx.doi.org/10.28991/CEJ-2024-010-09-09>



© 2024 by the authors. Licensee C.E.J, Tehran, Iran. This article is an open access article distributed under the terms and conditions of the Creative Commons Attribution (CC-BY) license (<http://creativecommons.org/licenses/by/4.0/>).

In order to optimize the performance of cross-sections with composite materials, these structures need to be analyzed and their shear stress distributions and deformations need to be assessed to obtain optimized designs. The effect of elements' thicknesses, widths, and material properties affects the overall torsional performance of the cross-section [2]. Thus, the sensitivity of these parameters needs to be evaluated to obtain an understanding of their effects. Extensive research effort has been devoted to deal with such problems [28–33], but neither has implemented these sensitivity studies through advanced sensitivity tools (e.g., Sobol's analysis with meta-modeling tools, such as Low-Rank Tensor Approximation) to assess the importance of each design parameter (i.e., input variable). Additionally, compared to traditional uniform structures, some researchers have incorporated graded properties, which have been shown to improve the energy-absorbing performance of thin-walled structures with various cross-sectional shapes [34, 35]. For example, beams with rectangular cross-sections have been optimized to create lightweight designs for real automobile structures while maintaining torsional stiffness [36]. Sensitivity analysis of rectangular tube cross-sections has also been used to inform the design of automobile frames [37]. Thin-walled beams (TWBs), typically formed by welding metal sheets, are crucial components of automobile frames and often have more complex cross-sectional shapes. Most research efforts have focused on simple forms like circular, rectangular, triangular, and basic cell shapes, with less attention given to optimizing more complex cross-sections for lightweight automobile frame designs. Moreover, these studies focused specifically on automobile applications; thus, the need for a generalized application and optimization process emerges.

The current study focuses on employing sensitivity tools on torsionally-loaded multicellular thin-walled cross-sections to obtain the relative importance of each parameter in the cross-section to the torsional performance of the whole structure. Key examples and applications are implemented to test the results of the sensitivity study and obtain optimized design recommendations. The results of the optimization process are compared with actual structural members used in real applications.

2. Theoretical Derivation of Torsional Properties

Gere & Goodno [1] presented the derivation of shear stresses in single-cell thin-walled isotropic tubes subjected to an external torque (T) as shown in Equation 1:

$$\tau = \frac{T}{2\Omega t} \xrightarrow{q=\tau t} q = \frac{T}{2\Omega} \quad (1)$$

where, τ is the shear stress, T is the torsional moment, Ω is the total area inside the centerline of the tube wall, t is the thickness of the tube wall, and q is the shear flow in the tube wall. Furthermore, the rate of twist (i.e., the angle of twist per unit length) of the member can be obtained by using Equation 2. Note that in Equation 2, the integral over the arc length can be approximated as a summation over multiple straight segments.

$$\theta = \frac{q}{2\Omega G} \oint \left(\frac{ds}{t}\right) \rightarrow \theta = \frac{T}{4\Omega^2 G} \oint \left(\frac{ds}{t}\right) \quad (2)$$

where, θ is the rate of twist ($\theta = \phi/L$), L is the member's length, ϕ is the angle of twist ($\phi = TL/GJ$), G is the shear modulus, J is the polar moment of inertia, and s is the arc length. From definition of the rate of twist and torsional stiffness (GJ/L), the polar moment of inertia (J) can be obtained using Equation 3:

$$\theta = \frac{T}{GJ} \rightarrow J = \frac{4\Omega^2}{\oint \left(\frac{ds}{t}\right)} \quad (3)$$

For multi-cellular thin-walled tubes, the general concept can be extended to obtain shear stresses and torsional stiffness. Oden & Ripperger [2] extended Equation 1 to get the equilibrium equation of a multi-cellular thin-walled tube under torsional moment as shown in Equation 4:

$$T = 2 \sum_{j=1}^N q_j \Omega_j \quad (4)$$

where, q_j is the shear flow in the j^{th} cell, Ω_j is the area enclosed by the centerline of the tube wall of the j^{th} cell, N is the number of cells. As shown in Figure 1, a three-celled section (i.e., i , j , and k) is used to illustrate the procedure for determining the shear stresses and the torsional stiffness of a three-cell thin-walled tube. Assuming that cell j is the only effective cell in the section and with using Equation 2, Equation 5 is obtained for the rate of twist of cell j . However, the assumption is based on the i^{th} and k^{th} cells having no shear flow. This assumption can be corrected by including the effect of the i^{th} and k^{th} cells, which results in Equation 6. Note that the shear flows are assumed to be positive in the counterclockwise direction for each of the cells (see Figure 1) and this results in the negative signs for the i^{th} and k^{th} cells in Equation 6:

$$\theta_j = \frac{q_j}{2G_j \Omega_j} \oint_{s_j} \left(\frac{ds}{t}\right) \quad (5)$$

where, θ_j is the rate of twist of the j^{th} cell, q_j is the shear flow in the j^{th} cell, G_j is the shear modulus of the j^{th} cell, Ω_j is the total area inside the centerline of the tube wall of the j^{th} cell, and s_j is the arc length of the j^{th} cell.

$$\theta_j = \frac{1}{2G_j\Omega_j} \left(q_j \oint_{s_j} \frac{ds}{t} - q_i \int_{s_{ji}} \frac{ds}{t} - q_k \int_{s_{jk}} \frac{ds}{t} \right) \tag{6}$$

where, q_i , q_j , and q_k are the shear flows in the i^{th} , j^{th} , and k^{th} cells, respectively, s_j is the arc length of the j^{th} cell, s_{ji} is the mutual arc length between the j^{th} and i^{th} cells, and s_{jk} is the mutual arc length between the j^{th} and k^{th} cells. Recalling that each of the cells does not distort in its own plane, but rather the whole cross section, and consequently each of the cells, rotate by the same rate of twist ($\theta_i = \theta_j = \theta_k = \theta$) [2].

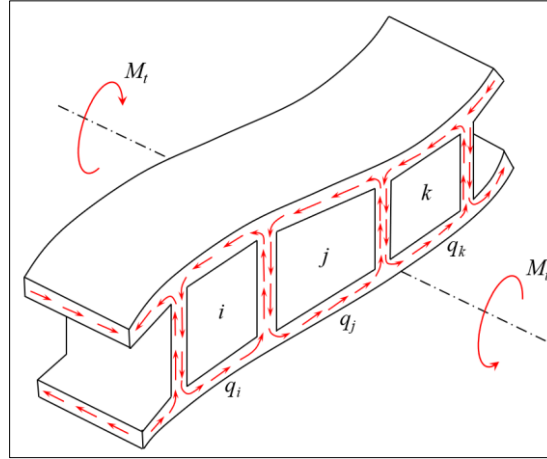


Figure 1. Multi-cellular tube in torsion (adapted from Oden & Ripperger [2])

Equation 7 is obtained for the case of the j^{th} cell being bounded by a total number of cells equal to m rather than two cells (i.e., i and k). This equation represents a set of equations called “equations of consistent deformation”. Note that the shear modulus is included inside the integral in case it is variable over the cross section.

$$\theta = \frac{1}{2\Omega_j} \left(q_j \oint_{s_j} \frac{ds}{Gt} - \sum_{r=1}^m \left(q_r \int_{s_{jr}} \frac{ds}{Gt} \right) \right) \tag{7}$$

where, m is the number of cells having boundaries with the j^{th} cell. With some algebraic manipulation, the equation of consistent deformation for the j^{th} cell is shown in Equation 8. The shear flow in each cell can be obtained by solving m -equations with m -unknowns simultaneously, this will calculate the shear flows in terms of the rate of twist of the whole cross section. Furthermore, by using Equation 4 (i.e., the equilibrium equation), the rate of twist, and consequently, the shear flows are determined. Then the shear stresses can be simply determined by multiplying the shear flows by the corresponding wall thicknesses.

$$\delta_{ji}q_i + \delta_{jj}q_j + \delta_{jk}q_k - 2\Omega_j\theta = 0 \tag{8}$$

where; $\left(\delta_{ji} = - \int_{s_{ji}} \frac{ds}{Gt} \right)$, $\left(\delta_{jj} = \oint_{s_j} \frac{ds}{Gt} \right)$, $\left(\delta_{jk} = - \int_{s_{jk}} \frac{ds}{Gt} \right)$, where, δ is the warping flexibilities. Finally, the torsional stiffness per unit length (GJ) can be obtained by using Equation 9 [2]:

$$GJ = \frac{2}{\theta} \sum_{j=1}^N q_j \Omega_j \tag{9}$$

Knowing that the torsional stiffness (or the torsional stiffness per unit length) is a cross-sectional and material-based property, there must be an alternative procedure to obtain these values without the need to go through the shear flows and the rate of twist calculations. Librescu & Song [38] introduced an equation (labelled as Equation 10 in this article) in which the cross-sectional stiffness, flexibility, and enclosed areas’ matrices are used to obtain the torsional stiffness per unit length (GJ) value of the whole cross section. Note that Equation 10 is essentially the same as the above-mentioned procedure with some algebraic manipulations to rather determine the GJ value directly from the input parameters. It is noteworthy to mention that the previous two procedures can be used for either a composite or a prismatic cross section, thus, the GJ value can be said to be the overall composite stiffness of the cross section.

$$GJ = 2\Omega^T S^{-1} \mathbf{I} \tag{10}$$

where:

$$\begin{aligned} S_{ji} &= \frac{1}{2\Omega_j} \delta_{ji} & S_{jj} &= \frac{1}{2\Omega_j} \delta_{jj} & S_{jk} &= \frac{1}{2\Omega_j} \delta_{jk} \\ S_{ii} &= \frac{1}{2\Omega_i} \delta_{ii} & S_{ij} &= \frac{1}{2\Omega_i} \delta_{ij} & S_{ik} &= \frac{1}{2\Omega_i} \delta_{ik} \\ S_{ki} &= \frac{1}{2\Omega_k} \delta_{ki} & S_{kj} &= \frac{1}{2\Omega_k} \delta_{kj} & S_{kk} &= \frac{1}{2\Omega_k} \delta_{kk} \end{aligned}$$

and, GJ is the torsional stiffness, and N is the number of cells, Ω^T is the transpose of the Ω matrix, and \mathbf{I} is the unit vector with the same order as the number of cells.

3. Sensitivity Analysis Theory

Sensitivity analysis helps in understanding how any change in the studied random input variables can have an influence on the output of the model. It can simplify complex problems in the reliability analysis, which includes probabilistic modeling [39]. This analysis shows how variations in input parameters affect the model's output variability [40] and identifies which variables are most influential. Thus, the input parameters of the model are split into random (i.e., most influential) and deterministic (i.e., other less influential) parameters [41, 42]. Additionally, sensitivity analysis also offers insights into how different inputs affect the model and measures changes in the output based on these inputs [39]. This is useful for optimizing structural designs and performing cost-benefit analyses by highlighting the most important variables [43].

Sensitivity analysis can be done in two main approaches: local and global [40, 44]. Local methods involve assessing the response of the model with changes in the input around a specific point, such as the average values of variables. An example of these methods is the first-order second-moments (FOSM) [39, 45]. These methods rely on linear approximations and provide sensitivity measures for that specific point. However, they may not capture the full picture. While global methods assess the sensitivity among all input variables and their ranges and can account for interactions between them [46]. For complex problems with many uncertain parameters, like the current case of study, local methods might not be sufficient because they only offer insight at a single point and may miss interactions that affect the overall behavior [46]. Therefore, global sensitivity analysis is often more appropriate for a comprehensive understanding and thus is the chosen approach for this study.

The global approach of the sensitivity analysis in its variance-based fashion measures quantitatively how the input parameters affect the output's variance [40]. It breaks down the output variance into parts and calculates how much each input parameter contributes to it [40]. This method is superior in its comprehensive assessment of the input space with its nonlinearity and interactions between its parameters. Sobol's method and the Fourier Amplitude Sensitivity Test (FAST) are among the widely used methods of the variance-based fashion of the sensitivity analysis [40]. FAST handles nonlinear relationships but doesn't account for interactions between parameters [40]. Thus, Sobol's method is used in this study for its effectiveness in dealing with complex systems that have significant nonlinearity and interactions [47].

3.1. Sobol Decomposition and Sobol's Sensitivity Indices

Let X represent the random vector containing the input parameters of the system and $F(X)$ be the response function within the n -dimensional unit cube k^n . This function can be expressed as [47]:

$$F(X) = F_0 + \sum_{1 \leq i \leq n} F_i(X_i) + \sum_{1 \leq i < j \leq n} F_{ij}(X_i, X_j) + \dots + F_{1 \dots n}(X_1, \dots, X_n) \quad (11)$$

where, X is the input vector having n random parameters, F_0 represents the average value of the response function, F_i is the portion of $F(X)$ that is influenced by the parameter X_i , and F_{ij} shows how the interaction between X_i and X_j affects $F(X)$. The right side of the equation (known as Sobol's functions) is determined by integrating the response function:

$$F_0 = \int_{k^n} F(x) dx \quad (12)$$

$$F_i(X_i) = \int_{k^{n-1}} F(x_{\sim i}, X_i) dx_{\sim i} - F_0 \quad (13)$$

$$F_{ij}(X_i, X_j) = \int_{k^{n-2}} F(x_{\sim ij}, X_i, X_j) dx_{\sim ij} - F_i(X_i) - F_j(X_j) - F_0 \quad (14)$$

In this context, $x_{\sim i}$ is a placeholder that shows the variable x_i is left out of the calculations. The term $\int_{k^{n-1}} F(x_{\sim i}, X_i) dx_{\sim i}$ represents an integration concerning all variables except X_i .

Knowing that Sobol's functions are orthogonal, so:

$$\int_{k^n} F_{i_1, i_2, \dots, i_s}(X_{i_1}, X_{i_2}, \dots, X_{i_s}) F_{j_1, j_2, \dots, j_s}(X_{j_1}, X_{j_2}, \dots, X_{j_s}) dx = 0 \quad (15)$$

As a result, the total variance D of $F(X)$ can be calculated as:

$$D = \text{Var}[F(X)] = \int_{k^n} F^2(X) dX - F_0^2 \quad (16)$$

In this case, input parameters are defined within an n -dimensional unit cube k^n . Through performing an integration of the square of Equation 11, the variance can be decomposed as:

$$D = \sum_{1 \leq i \leq n} D_i + \sum_{1 \leq i < j \leq n} D_{ij} + \dots + D_{1 \dots n} \quad (17)$$

$$D_i = \int_{k^1} F_i^2(X_i) dX_i \quad (18)$$

$$D_{ij} = \int_{k^2} F_{ij}^2(X_i, X_j) dX_i dX_j \quad (19)$$

In this context, D_i represents the partial variance related to the parameter X_i , D_{ij} is the partial variance caused by the interaction between parameters X_i and X_j , and $D_{1\ 2\ \dots\ n}$ represents the partial variance caused by the interaction among all parameters from X_1 to X_n . From these, Sobol's sensitivity indices can be calculated as:

$$S_i = \frac{D_i}{D} \quad (20)$$

$$S_{ij} = \frac{D_{ij}}{D} \quad (21)$$

In this case, S_i is the first-order sensitivity index, showing how much the output variance changes when only the i^{th} parameter is altered. Higher-order sensitivity indices, S_{ij} , reflect how interactions between multiple variables affect the output variance. Finally, the total Sobol's sensitivity index (S_i^T) for a parameter X_i combines both the first-order and higher-order sensitivity indices.

3.2. Sobol's Indices Using Low-Rank Tensor Approximation

Sobol's indices can be determined using Monte Carlo simulation [47], which involves sampling many different scenarios considering only one input variable (i.e., other are kept constant) and then estimating the variance uncertainty in the model's output. However, this approach can be costly because it requires a large number of simulations [40]. To address this, techniques that involve meta-modeling is employed to reduce computational costs. A meta-model is a simplified model that overruns the complex one in its fewer runs, but with similar results [48]. In order to achieve this, tools such as the Polynomial Chaos Expansion (PCE) and the Low-Rank Tensor Approximation (LRA) are used [49]. According to Konakli & Sudret [48], LRA converges more quickly to the exact solution and is better at predicting extreme responses compared to PCE. Therefore, this study will use sensitivity analysis in variance-based fashion combined with Low-Rank Tensor Approximation to evaluate how the variability in the input parameters (i.e., the geometric parameters and the mechanical properties) affects the overall torsional performance of multicellular thin-walled tubes.

In this paper, LRA is employed as the primary meta-modeling tool for sensitivity analysis. LRA is an efficient technique for approximating high-dimensional functions by decomposing them into lower-dimensional components. This approach significantly reduces the computational cost while maintaining high accuracy. The use of LRA allows for capturing non-linear interactions between input parameters, which is crucial for accurate sensitivity analysis. By integrating LRA with Sobol's method, a robust and efficient calculation of Sobol's indices is achieved, thereby enhancing the accuracy and reliability of the sensitivity analysis. The combination of LRA and Sobol's method ensures that the sensitivity indices reflect the real importance of each parameter, providing valuable insights for optimizing the design of multicellular thin-walled tubes.

4. Sensitivity Assessment Framework

The proposed sensitivity and optimization framework consists of two connected parts. Module I focused on assessing how different input parameters impact the structural behavior of multicellular thin-walled tubes. While Module II is tasked with finding the best shape (i.e., dimensions) for the structure. Module I begins by defining the statistical characteristics of the input variables, which include both geometric and mechanical parameters. Then, it performs a sensitivity analysis to pinpoint which parameters most significantly affect the multicellular thin-walled tube's performance and to explore how these parameters interact with each other.

In Module II, an optimization analysis was carried out with an emphasis on the sensitivity analysis results, the primary objective of this optimization analysis is to further enhance the overall torsional performance of multicellular thin-walled tubes through minimizing the rate of twist, improving the torsional stiffness, and limiting the shear stress (or shear flow). The non-dominated sorting genetic algorithm (NSGA-II) is utilized in this study to identify the best shape design. The optimization approach is then expanded to take into account the shape of the structure as well as material attributes. The input parameters (i.e., the width and thickness of each element) are optimized for several materials with an objective function to obtain the minimum mass of the structure that met some specific constraints related to the torsional performance of multicellular thin-walled tubes. Figure 2 shows a layout of the proposed framework. Moreover Figure 3 shows a flowchart identifying the process of the methodology.

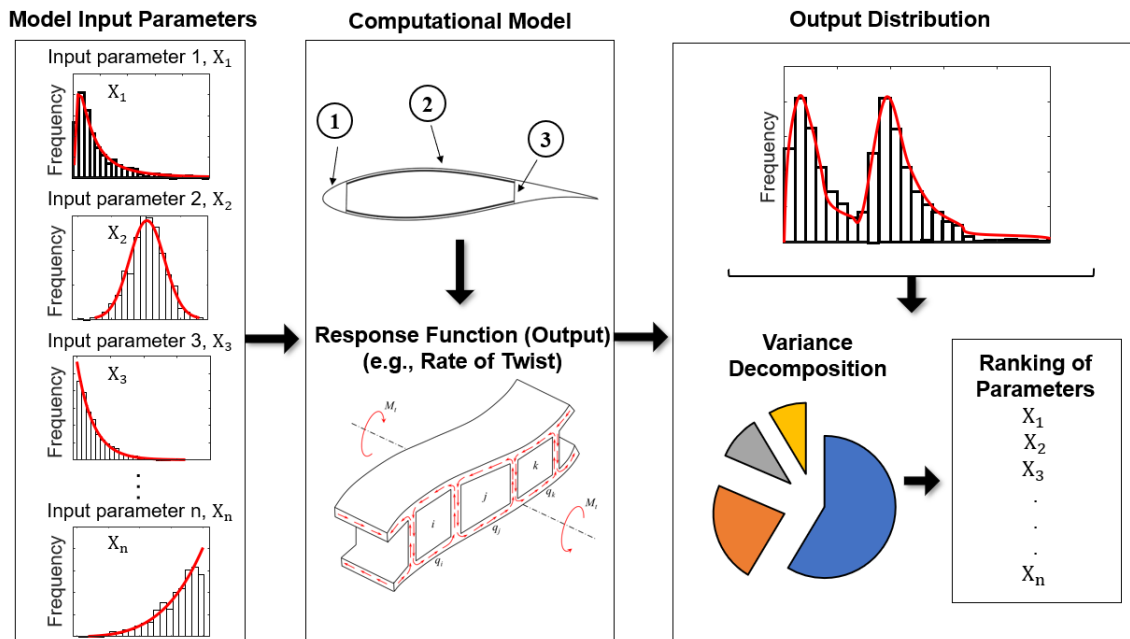


Figure 2. A schematic representation of the sensitivity analysis concept

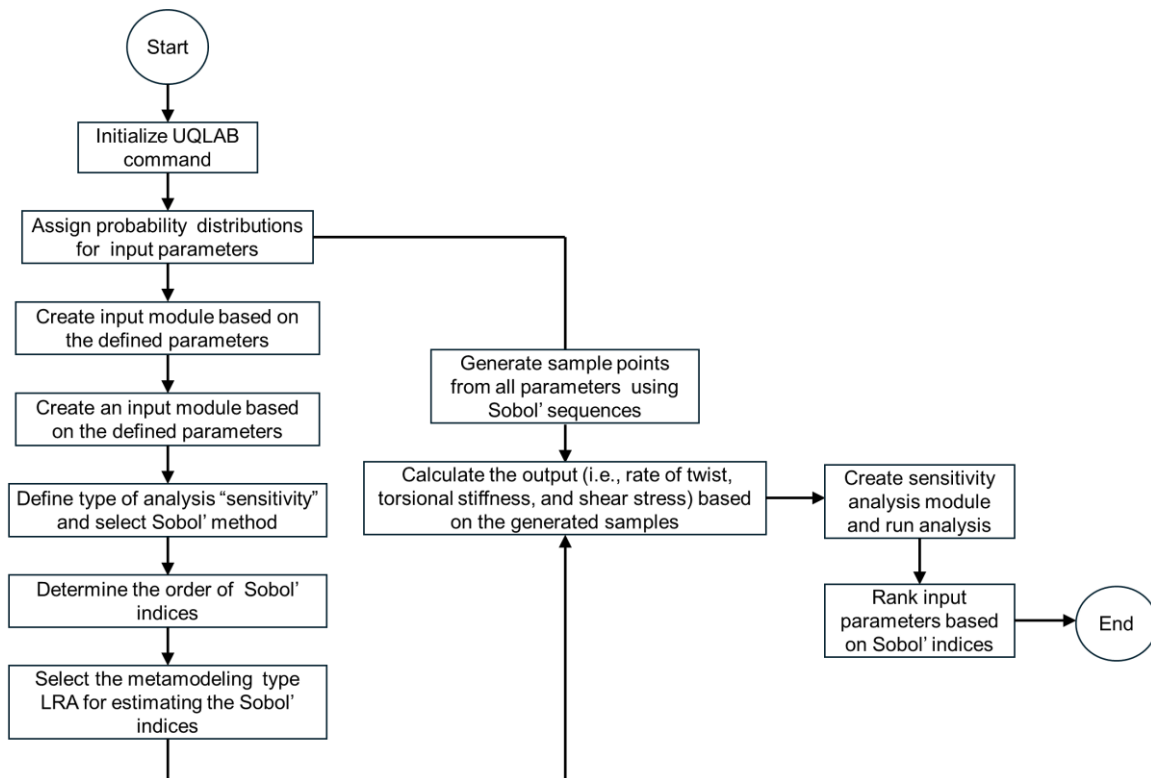


Figure 3. A flowchart of the sensitivity methodology

5. Analysis and Discussion

A sensitivity analysis is conducted using the Sobol method in combination with the LRA approximation tensor to identify crucial parameters that significantly impact the torsional performance of multicellular thin-walled tubes. The analysis conducted in this research focuses on tubes with three cells; the details of the thin-walled tube are shown in Figure 4, and it takes into account geometric parameters (such as beam length, thickness, and width) and mechanical properties (e.g., shear modulus) as input variables. The analysis and the obtained results can be extended to two or multicellular tubes (i.e., other than three). The response parameters, which describe the tubes' torsional characteristics, are calculated using Equations 4 and 7 to 10. The study evaluates the effects of the selected input variables (i.e., the geometric and the mechanical parameters) on the rate of twist, the torsional stiffness, and the maximum shear stress of the three-cell thin-walled tube.

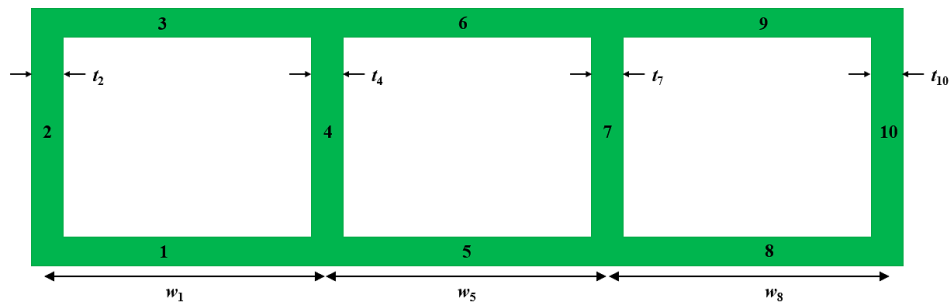


Figure 4. Elements labelling of the sample thin-walled tube studied

5.1. Illustrative Example

The shown example of a three-cell thin-walled tube in Figure 4 is used to investigate the effect of the constituents’ variability (i.e., input parameters) on the overall torsional performance.

5.1.1. Sensitivity Analysis of the Rate of Twist

Variance-based sensitivity analysis, combined with LRA, is employed to assess the influence of input parameter variability on the rate of twist, maximum shear stress, and torsional stiffness. A schematic representation of the developed sensitivity analysis concept can be seen in Figure 2. The UQ-Lab MATLAB toolbox is used to compute Sobol sensitivity indices for the variables considered [50, 51]. Based on convergence analysis results, 1,000 samples are drawn from each variable to obtain accurate Sobol indices using the distribution functions of input parameters presented in Table 1. Figures 5 and 6 show the sensitivity analysis results for the rate of twist as the primary output of interest. Figure 5 displays the total Sobol sensitivity indices for the geometric parameters (i.e., beam length, thickness, and width) and mechanical properties (i.e., shear modulus). As shown, the variability in the rate of twist depends heavily on the variability of the beam width, which contributes approximately 71% to the total variance. Shear modulus and beam thickness follow as the second and third dominant factors, with indices of 15% and 14%, respectively. In contrast, the variability in the length of the beam does not appear to contribute to the response variability, as indicated by its low sensitivity index of zero.

Table 1. Distribution functions of input parameters for sensitivity analysis

Input variable	Unit	Type of Distribution	Reference
Width (w)	mm	Normal (Gauss)	[52, 53]
Wall thickness (t)	mm	Normal (Gauss)	[52, 53]
Length (L)	m	Normal (Gauss)	[52, 53]
Shear modulus (G)	GPa	Normal (Gauss)	[52, 53]

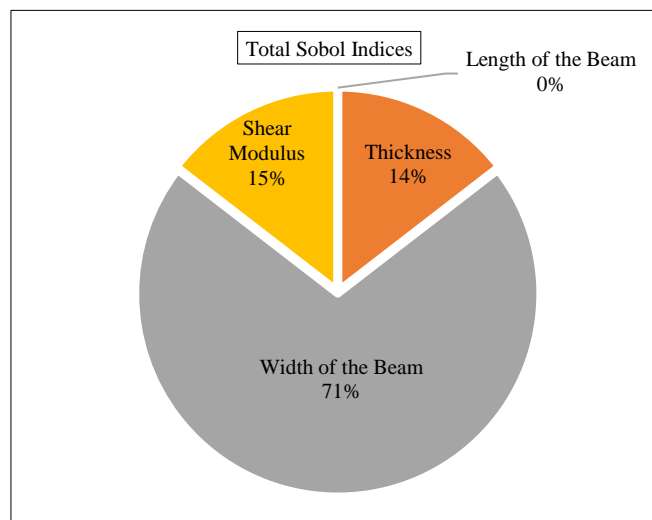


Figure 5. Sensitivity analysis results for the rate of twist as the primary output

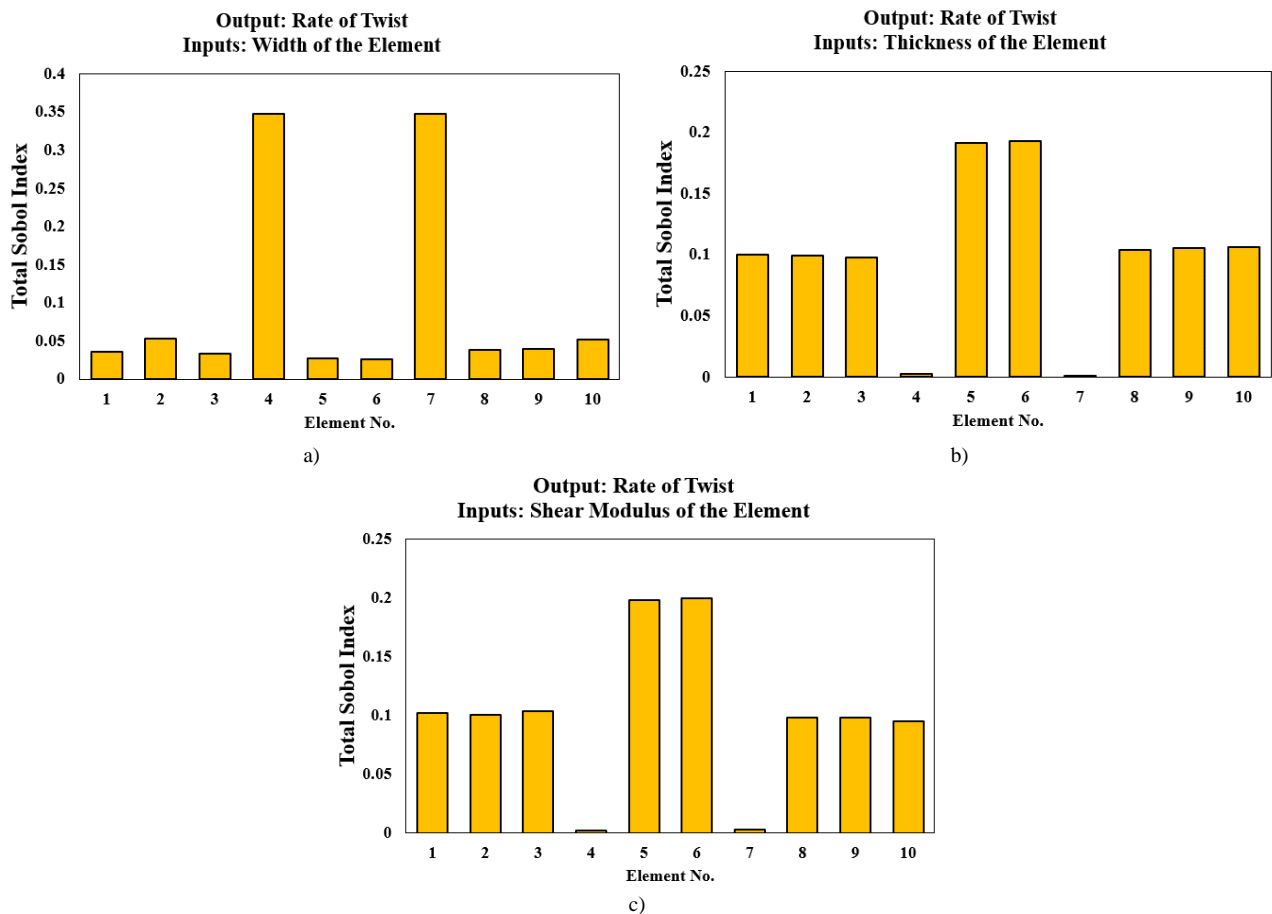


Figure 6. Sobol indices for each element and their effects on the variability of the rate of twist; a) the effect of element’s width, b) the effect of element’s thickness, and c) the effect of element’s shear modulus

Sobol indices for each element are then calculated to evaluate their individual effects on the variability of the rate of twist as shown in Figure 6. In Figure 6-a, the analysis reveals that the beam width, particularly for vertical elements, plays a predominant role in influencing variability in the rate of twist. Among the vertical elements, the interior ones (i.e., elements 4 and 7) and, to a lesser degree, the exterior ones (i.e., elements 2 and 10) exhibit a more significant impact on the rate of twist variability, indicating that alterations in their width are crucial for torsional performance. In contrast, the horizontal elements, both exterior (i.e., elements 1, 3, 8, and 9) and interior (i.e., elements 5 and 6), show a lower influence on the rate of twist variability.

Next, the effect of variability in the thickness of each element on the rate of twist is investigated by calculating the Sobol index associated with each element when thicknesses are the only variables. The total Sobol's sensitivity indices that represent the effect of the variability in the beam thickness for each element on the rate of twist are computed next and shown in Figure 6-b. The analysis shows that certain elements exhibit a higher influence on torsional behavior owing to the variation in thickness compared to others. Changes in thickness have a greater impact on the rate of twist variability for particular elements, such as the interior horizontal elements (i.e., elements 5 and 6). This indicates that these elements are more vulnerable to thickness variations, and altering their thickness can result in significant variations in torsional performance. In contrast, other elements, such as elements 4 and 7, have a considerably smaller influence on the rate of twist variability when their thickness is changed. This indicates that these elements are less vulnerable to thickness variations, therefore alterations to this parameter could not significantly alter the torsional behavior. Furthermore, the effect of shear modulus on the rate of twist varies among the elements as illustrated in Figure 6-c, with the interior horizontal elements (i.e., elements 5 and 6) demonstrating higher Sobol’s indices compared to their counterparts. This implies that these elements are more responsive to changes in shear modulus, which could substantially influence the torsional performance. These findings are consistent with the findings presented by Li & Easterbrook [11] and by Alhawamdeh et al. [54] and Yoo et al. [10] on the effect of geometric and material parameters on the rate of twist of multicellular thin-walled tubes. Moreover, Li & Easterbrook [11] state that if the cross-section is constructed using two materials with different shear moduli (i.e., one for the outside elements and one for the vertical mutual inside elements, these include elements 4 and 7), the angle of twist decrease with the increase in the ratio of the two shear moduli.

5.1.2. Sensitivity Analysis of the Maximum Shear Stress

The analysis in the previous section has been extended to investigate the effect of the stated input parameter variability on the maximum shear stress. Figures 7 and 8 display the sensitivity analysis results for maximum shear stress as the main output of interest. Figure 7 displays the total Sobol sensitivity indices for the geometric parameters (i.e., beam length, thickness, and width) and mechanical properties (i.e., shear modulus). As shown, the variability in maximum shear stress depends heavily on the variability of the beam width, which contributes approximately 77% to the total variance. The beam thickness is the second dominant quantity, with indices of 22%. In contrast, the variability in the length of the beam and the shear modulus does not appear to contribute to the response variability, as indicated by its low sensitivity index of approximately zero.

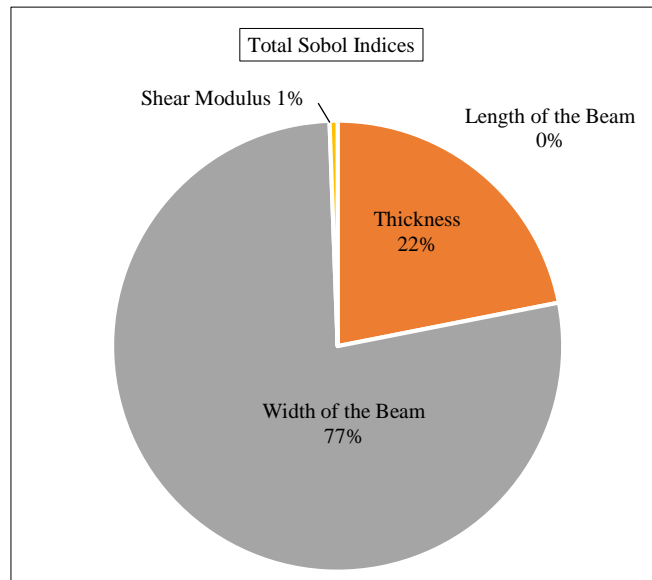


Figure 7. Sensitivity analysis results for the maximum shear stress as the primary output

Sobol indices for each element are computed to evaluate their individual effects on the variability of maximum shear stress, as illustrated in Figure 8. In Figure 8-a, the analysis emphasizes the prominent role of beam width, particularly for vertical elements, in influencing the variability of maximum shear stress. Among vertical elements, both interior (i.e., elements 4 and 7) and, to a lesser degree, exterior (i.e., elements 2 and 10) ones exhibit a more substantial impact on the maximum shear stress variability. This finding suggests that adjusting their width is critical to torsional performance. In contrast, horizontal elements, including exterior (i.e., elements 1, 3, 8, and 9) and interior (i.e., elements 5 and 6), display a lower influence on the maximum shear stress variability.

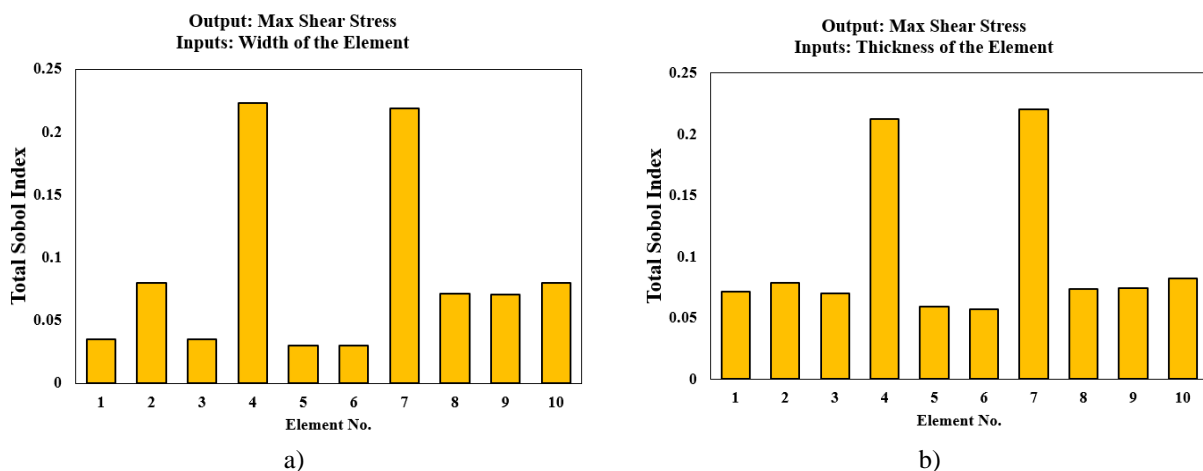


Figure 8. Sobol indices for each element and their effects on the variability of the maximum shear stress; a) the effect of element’s width, b) the effect of element’s thickness

Next, the effect of thickness variability of each element on maximum shear stress is investigated by calculating the associated Sobol index when only thicknesses are considered as variables. As shown in Figure 8-b, the analysis reveals that certain elements have a more significant impact on torsional behavior due to thickness changes than others. Similar

to the width variability, the vertical interior elements (i.e., elements 4 and 7) demonstrate a more pronounced influence on the maximum shear stress variability with thickness alterations. However, the effect of all other elements, except elements 5 and 6 which have a lesser effect, have a pronounced effect in reducing the maximum shear stress. This observation implies that torsional performance of all elements is sensitive to their thickness changes, and optimizing their thicknesses could lead to superior torsional performance. These findings are consistent with the findings presented by Li & Easterbrook [11] and by Alhawamdeh et al. [54] and Yoo et al. [10] on the effect of geometric and material parameters on the maximum shear stresses in multicellular thin-walled tubes. Moreover, Li & Easterbrook [11] states that if the cross-section is constructed using two materials with different shear moduli (i.e., one for the outside elements and one for the vertical mutual inside elements, these include elements 4 and 7), the shear stresses in the outside cells decrease with the increase in the ratio of the two shear moduli, while the shear stresses in the interior cell increase with the ratio of the two shear moduli

5.1.3. Sensitivity Analysis of the Torsional Stiffness

The sensitivity of the collective input parameters on torsional stiffness is also investigated by computing their Sobol indices. Figure 9 displays the total Sobol sensitivity indices for the geometric parameters (i.e., beam length, thickness, and width) and mechanical properties (i.e., shear modulus). As illustrated, the variability in torsional stiffness is heavily influenced by the variability of the width of the beam, which contributes approximately 68% to the total variance. Shear modulus and beam thickness follow as the second and third dominant factors, with equal indices of 16%. In contrast, the variability in the length of the beam does not appear to affect the response variability, as indicated by its negligible sensitivity index close to zero.

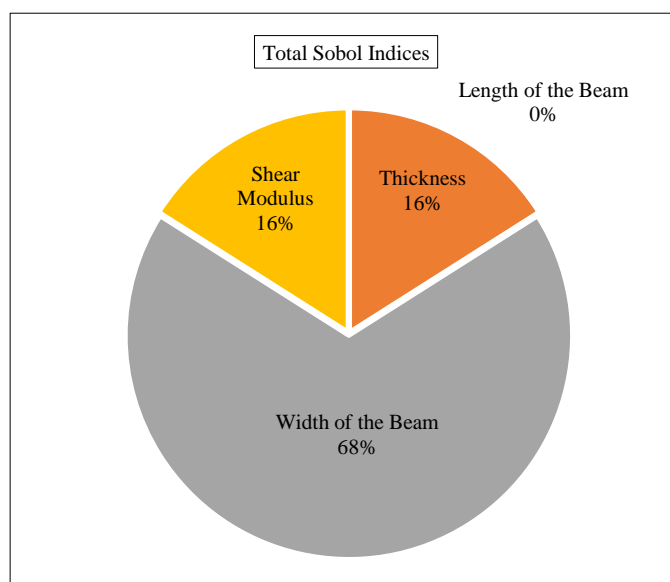


Figure 9. Sensitivity analysis results for the torsional stiffness as the primary output

The Sobol indices for each element are then calculated to evaluate their individual effects on the variability of torsional stiffness. The analysis highlights the influence of beam width, thickness, and shear stress on torsional stiffness across the various elements. Regarding beam width, as shown in Figure 10-a, the analysis reveals that the vertical interior elements (i.e., elements 4 and 7) display a greater impact on torsional stiffness variability compared to other elements. This suggests that adjusting the width of these specific vertical elements is crucial for optimizing torsional performance. Meanwhile, other elements, including horizontal elements (i.e., elements 1, 3, 5, 6, 8, and 9) and exterior vertical elements (i.e., elements 2 and 10), exhibit a relatively lower influence on the torsional stiffness variability.

Next, the effect of thickness variability on torsional stiffness is investigated. The calculated Sobol indices are shown in Figure 10-b. The analysis demonstrates that the interior horizontal elements (i.e., elements 5 and 6) have a more pronounced influence on torsional stiffness variability due to changes in thickness. This observation is also confirmed for the case of shear modulus variability (see Figure 10-c). This indicates that these specific elements are more sensitive to thickness and shear modulus changes, and modifying their thickness and shear moduli could lead to noticeable differences in torsional performance. Conversely, other elements, such as element 4 and element 7, show a relatively smaller impact on torsional stiffness variability when their thickness and shear moduli are altered. In conclusion, the torsional stiffness of multicellular thin-walled tubes is influenced by a combination of beam width, thickness, and shear modulus. This suggests that adjusting these parameters, particularly for specific vertical and horizontal interior elements, could lead to significant improvements in torsional performance. These findings are consistent with the findings

presented by Alhawamdeh et al. [54] for optimization of hollow box pultruded FRP profiles and Yoo et al. [10] for optimization of thin-walled cellular sections under the effect of geometric and material parameters on the optimized torsional stiffness in multicellular thin-walled tubes. Yoo et al. [10] results reveal that the finite element analysis (FEA) and the closed-form solution used, match the optimized design suggested herein to achieve maximum torsional stiffness.

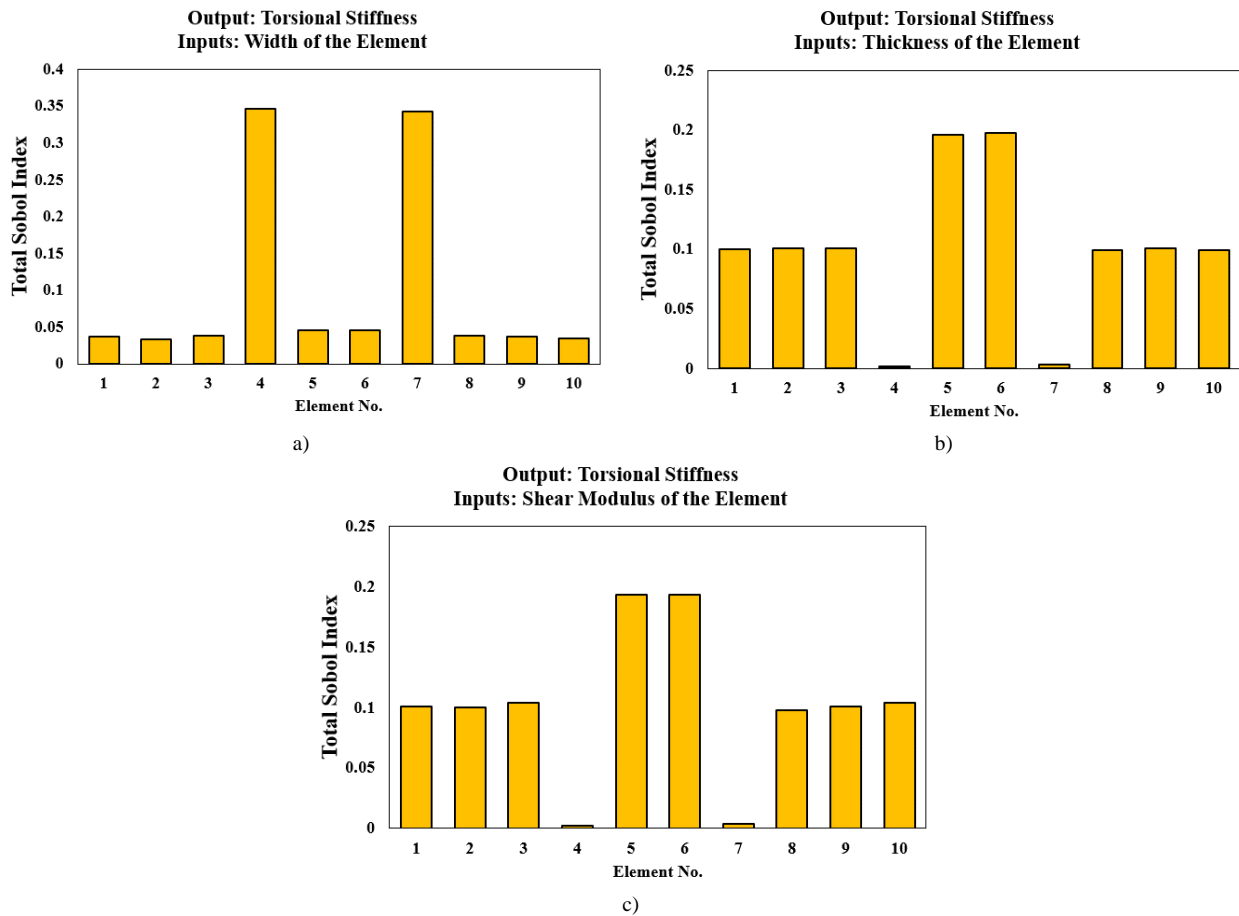


Figure 10. Sobol indices for each element and their effects on the variability of torsional stiffness; a) the effect of element’s width, b) the effect of element’s thickness, and c) the effect of element’s shear modulus

5.2. Thin-Walled Tube Optimization for Enhanced Torsional Performance

The conducted sensitivity analysis is useful for understanding the importance and interactions of various parameters affecting the torsional behavior of multicellular thin-walled tubes. It shows how uncertainties in the rate of twist, torsional stiffness, and maximum shear stress are influenced by different sources of uncertainties, but it doesn't directly measure how changes in one input parameter affect the output. To address this, an optimal shape design for the tubes is created using a multi-objective genetic algorithm (MOGA) to enhance torsional resistance. The non-dominated sorting genetic algorithm (NSGA-II) is employed in MATLAB to find the best solutions, with the key parameters of the MOGA listed in Table 2. For the optimization, the width and thickness of the tube elements are used as input parameters, and the process is constrained by a maximum area of 100,000 mm². The optimization procedure is performed with the goal of minimizing rate of twist, maximizing torsional stiffness, and minimizing shear stress.

Table 2. Main parameters used by MOGA

Input variable	Unit
Population size	150
Generation	60
Pareto fraction	0.4
Crossover fraction	0.8
Migration	0.2

The results of the optimization analysis are depicted in Figure 11, these results reveal helpful guidance for enhancing the torsional performance of multicellular thin-walled tubes. Figure 11-a depicts the situation with the rate of twist as

the output of interest, Figure 11-b focuses on torsional stiffness, and Figure 11-c investigates maximum shear stress. As shown, deeper vertical and thicker horizontal interior elements in the top-performing designs lead to superior torsional stiffness, reduce rate of twist, and a lower maximum shear stress, resulting in a superior shear performance overall. These findings are consistent with the sensitivity results, emphasizing the significance of precise geometric characteristics for reaching optimal tube design for enhanced performance. These findings provide valuable guidance for engineers and designers in the development of efficient and high-performance thin-walled tubes for various industrial applications. For example, the design of a Clipper C96 wind turbine blade’s cross section is shown in Figure 12 to compare it with the optimized design obtained herein (see Figure 11). As can be seen, the overall design consists of a thin aerodynamic shell, and thin and long vertical shear webs, and thick horizontal spar caps (note that the vertical shear webs and the aerodynamic shell are composed of sandwich structure intended for buckling resistance, but the composite material used is thin). Thus, this example illustrates how the design of wind blades is based on optimization tools that will produce a lightweight and structurally adequate structure, bearing in mind that the overall design of the wind blade’s cross section takes into account multiple design objectives (e.g., bending moments, torsional moments, axial and shear forces, and vibration) [55, 56].

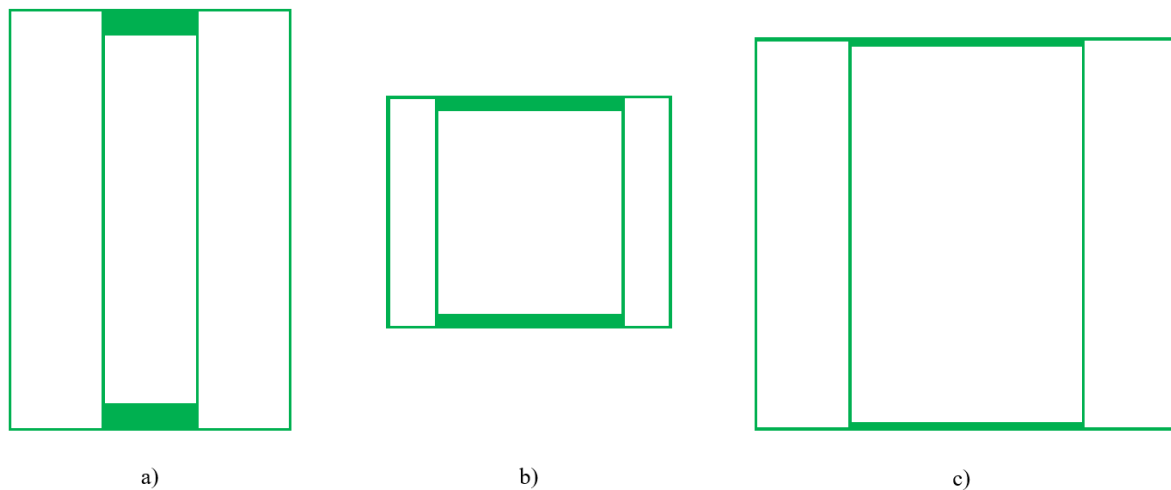


Figure 11. Optimal design configurations for three-cellular thin-walled tube; a) minimizing rate of twist, b) maximizing torsional stiffness, and c) minimizing shear stress

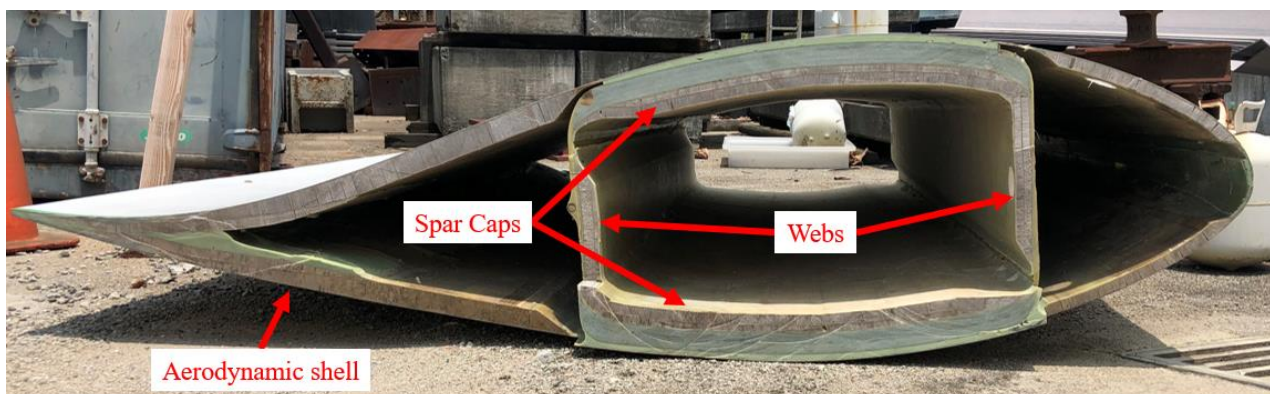


Figure 12. Clipper C96 wind turbine blade’s cross section

The optimization analysis is then extended to consider the material and shape of the structure. The analysis includes employing three categories of materials, which are identified in Table 3. The input parameters for the optimization process include the width and thickness of each element in the thin-walled structure. The maximum rate of twist, minimum torsional stiffness, and maximum shear stress are considered as the constraints utilized in the optimization process, and their thresholds are given in Table 4. The objective function attempts to minimize the mass of the structure based on the acquired dimensions (i.e., the width and thickness of each element) and the density of the chosen material. This procedure is executed for each material listed in Table 3. Subsequently, the optimal design is chosen based on the material that results in the minimum mass while satisfying the constraints. Note that shear moduli were calculated to be in the range of $E/3$ to $E/2$, where E is the Young’s modulus of the material [1].

Table 3. Characteristics for the different materials that were considered in the optimization analysis, including shear modulus, elastic modulus, and density (adapted from Ashby [57])

Material	E_{min} (GPa)	E_{max} (GPa)	G_{min} (GPa)	G_{max} (GPa)	Density (kg/m ³)	Cross-sectional Area (mm ²)	Mass (kg/m)
<i>Metals</i>							
Cast irons	170	180	57	90	7200	12817	92.3
High carbon steels	200	220	67	110	7850	10827	85.0
Medium carbon steels	200	220	67	110	7850	10827	85.0
Low carbon steels	200	220	67	110	7850	10827	85.0
Low alloy steels	210	220	70	110	7850	10629	83.4
Stainless steels	190	210	63	105	7850	11424	89.7
Aluminum alloys	68	82	23	41	2700	18320	49.5
Copper alloys	110	150	37	75	8900	15137	134.7
Lead alloys	13	15	4	8	10500	21768	228.6
Magnesium alloys	42	47	14	24	1850	20044	37.1
Nickel alloys	190	220	63	110	8900	11093	98.7
Titanium alloys	90	120	30	60	4600	16596	76.3
Zinc alloys	68	95	23	48	6000	17856	107.1
<i>Ceramics</i>							
Borosilicate glass	61	64	20	32	2250	19116	43.0
Silica glass	68	74	23	37	2200	18585	40.9
Soda-lime glass	68	72	23	36	2450	18652	45.7
Brick	15	30	5	15	1850	21238	39.3
Concrete	15	25	5	13	2450	21370	52.4
Stone	20	60	7	30	2300	20110	46.3
<i>Composites</i>							
Aluminum/silicon carbide	81	100	27	50	2780	17458	48.5
CFRP	69	150	23	75	1550	16066	24.9
GFRP	15	28	5	14	1900	21304	40.5

Table 3. The constraints utilized in the optimization process

Constraints	Value
Maximum rate of twist	0.01 rad/m
Minimum torsional stiffness	1.2×10^{12} N□mm
Maximum shear stress	16 MPa

Then, the optimal cross-sectional area of each material, as well as the mass of the structure, were obtained and shown in Table 3 and Figure 13. Among the metals, magnesium alloys had the lowest mass, at 37.1 kg/m, with a required cross-sectional area of 20,044 mm², leading to make it a possible lightweight alternative in this category. For ceramics, Silica glass had the lowest mass of 40.9 kg/m and the necessary cross-sectional area is 18,585 mm², this indicates that this material can be a potential for applications needing low mass and high stiffness. In the composites category, it is apparent that using CFRP yields the most attractive design since it had the lowest mass of just 24.9 kg/m and cross-sectional area of 16,066 mm², making it the best lightweight alternative among all categories. When comparing the three material categories (i.e., metals, ceramics, and composites), the composites group appears to provide the best balance of mass and the necessary cross-sectional area. Bearing in mind that the total cost might be another constraint, thus the use of ceramics (e.g., concrete) might be a more suitable selection for such constraints. This conclusion emphasizes the importance of material selection in achieving maximum structural performance while minimizing structure weight.

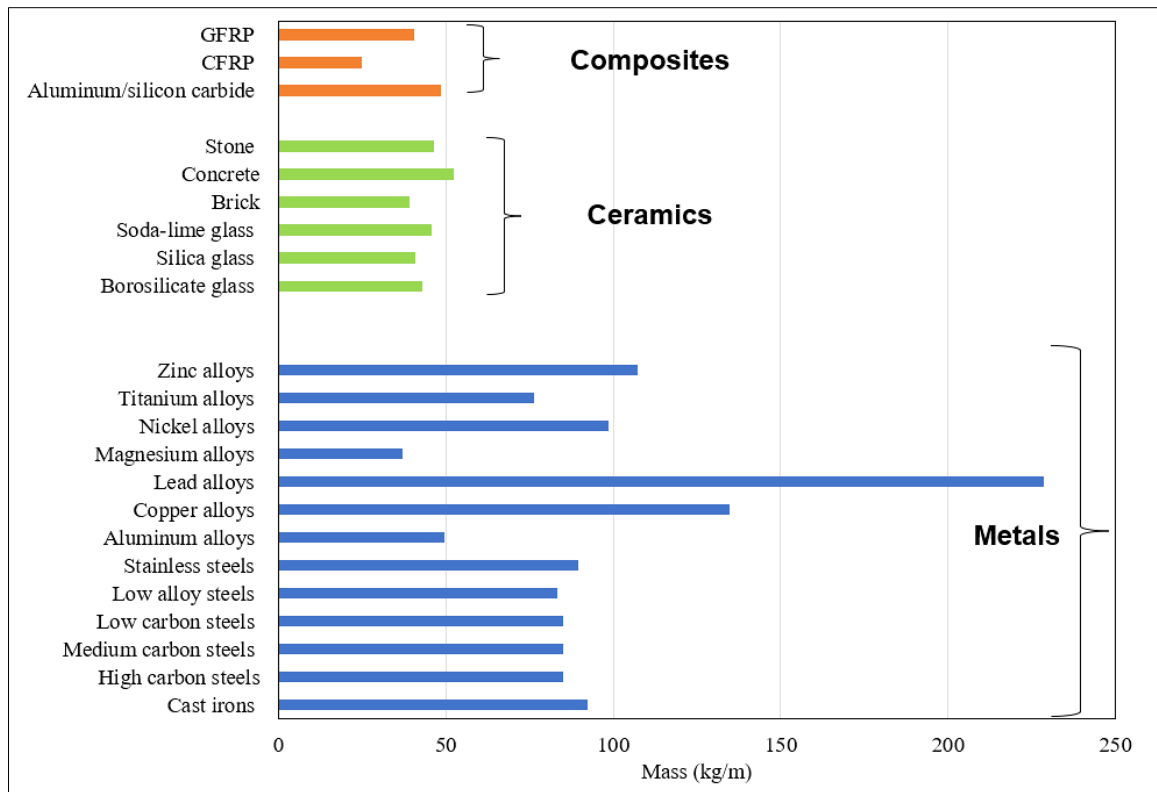


Figure 13. Mass per unit length that is needed for different materials in the optimized design

6. Conclusion

This study pinpointed the findings from analyzing and optimizing the torsional performance of multi-cellular thin-walled tubes. The sensitivity analysis was used to identify which key parameters most significantly affect the torsional performance and to find the optimal design for these thin-walled structures. The analysis took into account variations in both the mechanical properties and the geometric dimensions of the thin-walled structure. The sensitivity of the overall torsional performance (i.e., consisting of the rate of twist, the torsional stiffness, and the maximum shear stress or shear flow) for each of the input parameters provides a trade-off in the optimized design. For example, reducing the rate of twist in a three-cell thin-walled tube requires increasing the width of the interior vertical elements while increasing the thickness of all other elements. Thus, the optimized design will have interconnected relations between various elements to obtain the desired properties.

The optimal design of a three-cell thin-walled tube consists of using deeper vertical and thicker horizontal interior elements leading to superior torsional stiffness, a reduced rate of twist, and a minimized maximum shear stress. These findings are consistent with the widely used design of wind turbine blades where thick spar caps (i.e., horizontal interior elements) and thin aerodynamic shells (i.e., exterior elements) and vertical webs (i.e., vertical interior elements) are used. Thus, emphasizing the significance of precise geometric characteristics for reaching optimal thin-walled tube design for enhanced torsional performance. Optimization of the cross-section of the tube by considering the material and the shape of the structure results in a more attractive design bearing in mind that the mass or the cost of the structure might provide an additional constraint. By considering the design to be controlled by maximizing shear stiffness, minimizing mass, and minimizing maximum shear stress and rate of twist, optimal designs were obtained in the categories of composite materials and ceramics rather than metals. Furthermore, the composites group appears to provide the best balance of mass and the necessary cross-sectional area. If the cost is sought to be minimal, ceramics (e.g., concrete) might be a more suitable selection for such constraints.

7. Declarations

7.1. Author Contributions

Conceptualization, A.A.A., M.F.T., and M.I.A.; methodology, A.A.A. and M.F.T.; software, A.A.A. and M.F.T.; validation, A.A.A., M.F.T., and M.I.A.; formal analysis, A.A.A., M.F.T., and M.I.A.; investigation, A.A.A. and M.F.T.; resources, A.A.A. and M.F.T.; data curation, A.A.A. and M.F.T.; writing—original draft preparation, A.A.A. and M.F.T.; writing—review and editing, A.A.A., M.F.T., and M.I.A.; visualization, A.A.A. and M.F.T.; supervision, A.A.A., M.F.T., and M.I.A.; project administration, A.A.A., M.F.T., and M.I.A.; funding acquisition, A.A.A., M.F.T., and M.I.A. All authors have read and agreed to the published version of the manuscript.

7.2. Data Availability Statement

The data presented in this study are available on request from the corresponding author.

7.3. Funding

The authors received no financial support for the research, authorship, and/or publication of this article.

7.4. Conflicts of Interest

The authors declare no conflict of interest.

8. Nomenclature

D =	Total variance;	$D_{12\dots n}$ =	Partial variance due to the interaction between parameters X_1 to X_n ;
D_i =	Partial variance of parameter X_i ;	D_{ij} =	Partial variance due to the interaction between parameters X_i and X_j ;
E_{max} =	Maximum Young's modulus;	E_{min} =	Minimum Young's modulus;
$F(\mathbf{X})$ =	Response function within the n -dimensional unit cube k^n ;	F_o =	Average value of the response function $F(\mathbf{X})$;
F_i =	The part of $F(\mathbf{X})$ affected by parameter X_i ;	F_{ij} =	The part of $F(\mathbf{X})$ resulting from the interaction between X_i and X_j ;
G =	Shear modulus;	G_j =	Shear modulus of the j^{th} cell;
G_{max} =	Maximum shear modulus;	G_{min} =	Minimum shear modulus;
GJ =	Torsional stiffness;	\mathbf{l} =	The unit vector with the same order as the number of cells;
J =	Polar moment of inertia;	k^n =	Unit cube with n -dimensions;
L =	Member's length;	m =	Number of cells having boundaries with the j^{th} cell;
N =	Number of cells;	n =	Number of random parameters;
q =	Shear flow in the tube wall;	q_j =	Shear flow in the j^{th} cell;
S_i =	First-order sensitivity index;	S_{ij} =	Higher-order sensitivity indices;
S_i^T =	Total Sobol's sensitivity index one parameter X_i ;	s =	Arc length;
s_j =	Arc length of the j^{th} cell;	s_{ji} =	The mutual arc length between the j^{th} and i^{th} cells;
s_{jk} =	The mutual arc length between the j^{th} and k^{th} cells;	T =	Torsional moment;
t =	Thickness of the tube wall;	w =	Width of the element;
\mathbf{X} =	Random vector of system input parameters;	X_i =	i^{th} input variable;
x_{-i} =	Placeholder that shows the variable x_i is left out of the calculations;	δ =	Warping flexibilities;
Ω =	Total area enclosed by the centerline of the tube wall;	Ω_j =	Area enclosed by the centerline of the tube wall of the j^{th} cell;
Ω^T =	Transpose of the Ω matrix;	ϕ =	Angle of twist;
τ =	Shear stress;	θ =	Rate of twist;
θ_j =	Rate of twist of the j^{th} cell;		

9. References

- [1] Gere, J. M., & Goodno, B. J. (2017). *Mechanics of Materials*. Cengage Learning, Massachusetts, United States.
- [2] Oden, J., & Ripperger, E. (1981). *Mechanics of elastic structures*. Hemisphere Publishing Corp, Washington, United States.
- [3] Philippidis, T. P., Vassilopoulos, A. P., Katopis, K. G., & Voutsinas, S. G. (1996). THIN/PROBEAM: A software for fatigue design and analysis of composite rotor blades. *Wind Engineering*, 20(5), 349–362.
- [4] Jönsson, J. (1998). Determination of shear stresses, warping functions and section properties of thin-walled beams using finite elements. *Computers and Structures*, 68(4), 393–410. doi:10.1016/S0045-7949(98)00070-4.
- [5] Tariq, M. M., & Ahmed, M. N. (2010). Software development for shear stress distribution in multicell beams of isotropic materials. *Key Engineering Materials*, 442, 453–461. doi:10.4028/www.scientific.net/KEM.442.453.
- [6] Boresi, A. P., & Schmidt, R. J. (2002). *Advanced mechanics of materials*. John Wiley & Sons, Hoboken, United States.
- [7] Waldron, P. (1986). Sectorial properties of straight thin-walled beams. *Computers and Structures*, 24(1), 147–156. doi:10.1016/0045-7949(86)90344-5.
- [8] Chai Hong Yoo, & Acra, S. V. (1986). Cross-sectional properties of thin-walled multi-cellular section. *Computers and Structures*, 22(1), 53–61. doi:10.1016/0045-7949(86)90084-2.
- [9] Johnson, D. (1988). A Cellular Analogy for the Saint- Venant Torsion Analysis of Solid and Hollow Sections. *Computer-Aided Civil and Infrastructure Engineering*, 3(2), 173–178. doi:10.1111/j.1467-8667.1988.tb00167.x.

- [10] Yoo, C. H., Kang, J., Kim, K., & Lee, K. C. (2011). Shear flow in thin-walled cellular sections. *Thin-Walled Structures*, 49(11), 1341–1347. doi:10.1016/j.tws.2011.02.014.
- [11] Li, L. Y., & Easterbrook, D. (2014). Free torsion of thin-walled structural members of open- and closed-sections. *Applied Mathematics and Mechanics*, 35(1), 25–32. doi:10.1007/s10483-014-1769-6.
- [12] Gebre, T. H., Galishnikova, V. V., Lebed, E. V., & Tupikova, E. M. (2023). Modelling of thin-walled members with restrained torsion considering the section properties. *Magazine of Civil Engineering*, 118(2), 11806. doi:10.34910/MCE.118.6.
- [13] He, H. N., Wang, S. Y., Xi, H. F., Xiao, H., Zhan, L., & Zhou, J. S. (2024). The large strain snap-through effect in free torsion of highly elastic soft, thin-walled tubes with exact closed-form solutions. *Thin-Walled Structures*, 199, 111803. doi:10.1016/j.tws.2024.111803.
- [14] Rees, D. W. A., & Alsheikh, A. M. S. (2024). Theory of Flexural Shear, Bending and Torsion for a Thin-Walled Beam of Open Section. *World Journal of Mechanics*, 14(03), 23–53. doi:10.4236/wjm.2024.143003.
- [15] Bank, L. C. (2006). *Composites for Construction: Structural Design with FRP Materials*. Wiley, Hoboken, United States. doi:10.1002/9780470121429.
- [16] Han, M. L., Wang, H. Y., Wang, S. Y., & Xiao, H. (2023). Exact large strain analysis for the Poynting effect of freely twisted thin-walled tubes made of highly elastic soft materials. *Thin-Walled Structures*, 184, 110503. doi:10.1016/j.tws.2022.110503.
- [17] Li, B. F., Wang, X. T., Lv, B. H., Yan, X. F., & Yan, C. Z. (2023). Experimental study on torsional behavior of tapered high strength thin-walled concrete-filled double-skin steel tubular columns. *Structures*, 55, 1823–1838. doi:10.1016/j.istruc.2023.07.001.
- [18] Weber, D. E., Graupner, N., & Müssig, J. (2023). Manufacturing of flax- and glass-fibre reinforced thin-walled tubes and measuring their interlaminar shear properties by torsion tests. *Composite Structures*, 319, 117191. doi:10.1016/j.compstruct.2023.117191.
- [19] Chandra, R., Stemple, A. D., & Chopra, I. (1990). Thin-walled composite beams under bending, torsional, and extensional loads. *Journal of Aircraft*, 27(7), 619–626. doi:10.2514/3.25331.
- [20] Salim, H. A. (1996). *Modeling and application of thin-walled composite beams in bending and torsion*. PhD Thesis, West Virginia University, Morgantown, United States.
- [21] Volovoi, V. V., & Hodges, D. H. (2002). Single- and multicelled composite thin-walled beams. *AIAA Journal*, 40(5), 960–965. doi:10.2514/2.1733.
- [22] Jung, S. N., Park, I. J., & Shin, E. S. (2007). Theory of thin-walled composite beams with single and double-cell sections. *Composites Part B: Engineering*, 38(2), 182–192. doi:10.1016/j.compositesb.2006.07.001.
- [23] Loughlan, J., & Ahmed, M. N. (2008). Multi-cell carbon fibre composite box beams subjected to torsion with variable twist. *Thin-Walled Structures*, 46(7–9), 914–924. doi:10.1016/j.tws.2008.01.010.
- [24] da Silva, G. F., Marín, J. C., & Barroso, A. (2011). Evaluation of shear flow in composite wind turbine blades. *Composite Structures*, 93(7), 1832–1841. doi:10.1016/j.compstruct.2011.02.002.
- [25] Rajagopalan, K. (2022). *Torsion of Thin Walled Structures*. Springer Nature, Singapore. doi:10.1007/978-981-16-7458-7.
- [26] Alshannaq, A. A., Bank, L. C., Scott, D. W., & Gentry, T. R. (2021). Structural Analysis of a Wind Turbine Blade Repurposed as an Electrical Transmission Pole. *Journal of Composites for Construction*, 25(4), 4021023. doi:10.1061/(asce)cc.1943-5614.0001136.
- [27] Dababneh, O., & Kayran, A. (2014). Design, analysis and optimization of thin walled semi-monocoque wing structures using different structural idealization in the preliminary design phase. *International Journal of Structural Integrity*, 5(3), 214–226. doi:10.1108/IJSI-12-2013-0050.
- [28] Bank, L. C., & Bednarczyk, P. J. (1988). A beam theory for thin-walled composite beams. *Composites Science and Technology*, 32(4), 265–277. doi:10.1016/0266-3538(88)90065-6.
- [29] Bank, L. C., & Kao, C. H. (1989). The influence of geometric and material design variables on the free vibration of thin-walled composite material beams. *Journal of Vibration and Acoustics*, 111(3), 290–297. doi:10.1115/1.3269855.
- [30] Budkowska, B. B., & Szymczak, C. (1991). Sensitivity analysis of thin-walled I-beams undergoing torsion. *Thin-Walled Structures*, 12(1), 51–61. doi:10.1016/0263-8231(91)90026-F.
- [31] Szymczak, C., Kreja, I., Mikulski, T., & Kujawa, M. (2003). *Sensitivity Analysis of Beams and Frames Made of Thin-Walled Members*. Gdansk University of Technology, Gdansk, Poland.
- [32] Szymczak, C. (2003). Sensitivity analysis of thin-walled members, problems and applications. *Thin-Walled Structures*, 41(2–3), 271–290. doi:10.1016/S0263-8231(02)00091-5.
- [33] Ma, Y., Wang, X., & Zuo, W. (2020). Analytical Sensitivity Analysis Method of Cross-Sectional Shape for Thin-Walled Automobile Frame Considering Global Performances. *International Journal of Automotive Technology*, 21(5), 1207–1216. doi:10.1007/s12239-020-0114-8.

- [34] Xu, F., Zhang, X., & Zhang, H. (2018). A review on functionally graded structures and materials for energy absorption. *Engineering Structures*, 171, 309–325. doi:10.1016/j.engstruct.2018.05.094.
- [35] Zhou, L., Ren, S., Liu, C., & Ma, Z. (2019). A valid inhomogeneous cell-based smoothed finite element model for the transient characteristics of functionally graded magneto-electro-elastic structures. *Composite Structures*, 208, 298–313. doi:10.1016/j.compstruct.2018.09.074.
- [36] Zhou, L., Ren, S., Meng, G., & Ma, Z. (2020). Node-based smoothed radial point interpolation method for electromagnetic-thermal coupled analysis. *Applied Mathematical Modelling*, 78, 841–862. doi:10.1016/j.apm.2019.09.047.
- [37] Chen, W., & Zuo, W. (2014). Component sensitivity analysis of conceptual vehicle body for lightweight design under static and dynamic stiffness demands. *International Journal of Vehicle Design*, 66(2), 107–123. doi:10.1504/IJVD.2014.064546.
- [38] Librescu, L., & Song, O. (2005). *Thin-walled composite beams: theory and application*. Springer, Dordrecht, Netherland.
- [39] Gaspar, B., Teixeira, A., & Soares, C. (2016). *Sensitivity analysis of the IACS-CSR buckling strength requirements for stiffened panels*. Maritime Technology and Engineering, CRC Press, London, United Kingdom. doi:10.1201/b21890-62.
- [40] Saltelli, A., Annoni, P., Azzini, I., Campolongo, F., Ratto, M., & Tarantola, S. (2010). Variance based sensitivity analysis of model output. Design and estimator for the total sensitivity index. *Computer Physics Communications*, 181(2), 259–270. doi:10.1016/j.cpc.2009.09.018.
- [41] Opgenoord, M. M. J., Allaire, D. L., & Willcox, K. E. (2016). Variance-based sensitivity analysis to support simulation-based design under uncertainty. *Journal of Mechanical Design*, 138(11), 111410. doi:10.1115/1.4034224.
- [42] Khandel, O., Tamimi, M. F., Soliman, M., Russell, B. W., & Waite, C. D. (2022). Reliability assessment of connections with slip-critical bolts and fillet welds in combination. *Journal of Constructional Steel Research*, 188, 107036. doi:10.1016/j.jcsr.2021.107036.
- [43] Leheta, H. W., & Mansour, A. E. (1997). Reliability-based method for optimal structural design of stiffened panels. *Marine Structures*, 10(5), 323–352. doi:10.1016/s0951-8339(96)00026-3.
- [44] Sudret, B. (2008). Global sensitivity analysis using polynomial chaos expansions. *Reliability Engineering and System Safety*, 93(7), 964–979. doi:10.1016/j.res.2007.04.002.
- [45] Castillo, E., Fernández-Canteli, A., Hadi, A. S., & López-Aenlle, M. (2007). A fatigue model with local sensitivity analysis. *Fatigue & Fracture of Engineering Materials and Structures*, 30(2), 149–168. doi:10.1111/j.1460-2695.2006.01099.x.
- [46] Velarde, J., Kramhøft, C., & Sørensen, J. D. (2019). Global sensitivity analysis of offshore wind turbine foundation fatigue loads. *Renewable Energy*, 140, 177–189. doi:10.1016/j.renene.2019.03.055.
- [47] Sobol, I. M. (2001). Global sensitivity indices for nonlinear mathematical models and their Monte Carlo estimates. *Mathematics and Computers in Simulation*, 55(1–3), 271–280. doi:10.1016/S0378-4754(00)00270-6.
- [48] Konakli, K., & Sudret, B. (2016). Polynomial meta-models with canonical low-rank approximations: Numerical insights and comparison to sparse polynomial chaos expansions. *Journal of Computational Physics*, 321, 1144–1169. doi:10.1016/j.jcp.2016.06.005.
- [49] Janon, A., Klein, T., Lagnoux, A., Nodet, M., & Prieur, C. (2014). Asymptotic normality and efficiency of two Sobol index estimators. *ESAIM: Probability and Statistics*, 18, 342–364. doi:10.1051/ps/2013040.
- [50] Marelli, S., & Sudret, B. (2014). UQLab: A Framework for Uncertainty Quantification in Matlab. *Vulnerability, uncertainty, and risk: quantification, mitigation, and management*, 2554–2563, American Society of Civil Engineers (ASCE), Reston, United States. doi:10.1061/9780784413609.257.
- [51] MATLAB-MathWorks. (2022). MATLAB: MathWorks, Inc. Natick, United States. Available online: <https://www.mathworks.com/products/matlab.html> (accessed on July 2024).
- [52] Kala, Z. (2005). Sensitivity analysis of the stability problems of thin-walled structures. *Journal of Constructional Steel Research*, 61(3), 415–422. doi:10.1016/j.jcsr.2004.08.005.
- [53] Kotelko, M., Lis, P., & Macdonald, M. (2017). Load capacity probabilistic sensitivity analysis of thin-walled beams. *Thin-Walled Structures*, 115, 142–153. doi:10.1016/j.tws.2017.02.007.
- [54] Alhawamdeh, M., Alajarmeh, O., Aravinthan, T., Shelley, T., Schubel, P., Mohammed, A., & Zeng, X. (2022). Design optimisation of hollow box pultruded FRP profiles using mixed integer constrained Genetic algorithm. *Composite Structures*, 302, 116247. doi:10.1016/j.compstruct.2022.116247.
- [55] Veers, P. S., Ashwill, T. D., Sutherland, H. J., Laird, D. L., Lobitz, D. W., Griffin, D. A., Mandell, J. F., Músiál, W. D., Jackson, K., Zuteck, M., Miravete, A., Tsai, S. W., & Richmond, J. L. (2003). Trends in the design, manufacture and evaluation of wind turbine blades. *Wind Energy*, 6(3), 245–259. doi:10.1002/we.90.
- [56] Schubel, P. J., & Crossley, R. J. (2012). Wind turbine blade design. *Energies*, 5(9), 3425–3449. doi:10.3390/en5093425.
- [57] Ashby, M. F. (1994). *Materials selection in mechanical design*. Metallurgia Italiana, 86, 475–475.